SPIN-LABEL STUDIES OF ERYTHROCYTE DEFORMABILITY

IV. Relation of Electron Spin Resonance Spectral Change with Deformation and Orientation of Erythrocytes in Shear Flow

SUMIHARE NOJI AND HIDEO KON
Laboratory of Chemical Physics, National Institute of Arthritis, Diabetes and Digestive and Kidney Diseases, National Institutes of Health, Bethesda, Maryland 20205

SHIGEHIKO TANIGUCHI
Department of Biochemistry, Okayama University Dental School, Okayama 700, Japan

ABSTRACT Electron spin resonance (ESR) spectra of spin-labeled human erythrocytes in shear flow are simulated to derive semi-empirical relations of the ESR spectral change with deformation and orientation of the cells by using a modified theoretical model developed for deformation and orientation of liquid drops. The six observed spectra at different shear stress values were simultaneously simulated by adjusting only two parameters. One parameter can be related to the ratio of the internal to the external viscosity, and the other to the elastic property of the cell membrane. From these results we have derived a semi-empirical relationship between the average deformation index or the orientation angle with a spectral measure, which characterizes the spectral shape change induced by shear stress. Thus, it becomes possible to obtain improved quantitative information on the rheological behavior of red blood cells by using the spin-label ESR method.

INTRODUCTION

The ability of normal human erythrocytes to deform in blood flow is an essential factor for their function and survival, since they must negotiate their way through capillaries and the narrow portals of the spleen. For example, it has been suggested that when this ability is lost in vivo for any reason, the red blood cells are trapped between the splenic cords and destroyed (1). In fact, premature destruction of red cells due to reduced deformability was observed in several diseases such as Duchenne muscular dystrophy as reported by Rice-Evans and Dunn (1). It is, thus, quite important clinically and biophysically to elucidate the mechanisms by which the red cells exhibit the extraordinary deformability without losing their structural integrity.

Recently, we have expanded the application of the electron spin resonance (ESR) spin-labeling method to assess the deformation of the red cells in shear flow by measuring the ESR spectral change induced by the flow, and also by observing the recovery process of the spectral difference when the flow is abruptly interrupted (2–4). In the previous papers of this series (2, 4), we demonstrated that the change of the spectra by shear stress reflects the extent of both the whole cell deformation and orientation, which depend upon the intrinsic as well as the extrinsic mechanical properties of the cells.

Furthermore, it was confirmed by photomicrographic observation that under the same conditions as in the ESR experiments, the cells in flow were elongated and aligned approximately along the flow direction (4). Based upon these results, we attempt here to extract more quantitative information from the ESR spectral change by simulating the ESR spectra observed at various shear stress values.

Recently, Bitbol and Leterrier (5) reported the simulation of the ESR spectra of red cells in shear flow with the assumption that the cells orient without deformation. As has been well demonstrated (2, 4, 6, 7), however, the red cell orientation in flow is closely tied to simultaneous deformation, and if the cells are hardened, they rotate in flow and do not orient. This assumption of no deformation, therefore, is not applicable to most cases in which orientation is accompanied by the cell deformation. It may be

---

This article is dedicated to Dr. Ulrich Weiss on the occasion of his 75th birthday.

S. Noji's present address is the Department of Biochemistry, Okayama University Dental School, 2-5-1 Shikatacho, Okayama 700, Japan.

Address all reprint requests to H. Kon, Room B1-14, Bldg. 2, NIH, Bethesda, MD 20205.

justified in situations of low shear rate flow in which the cells retain a nearly biconcave shape and orient to some extent, but would not apply to the high shear rate conditions.

The general procedure for simulation of the ESR spectra of spin-labeled fatty acid incorporated in a lipid matrix has been well established (8). The remaining problem in simulation is how to describe the deformation and orientation of the cells in flow. Since, in the ESR experiments, a flat quartz cell with a small gap between the surfaces was used as a flow cell, the flow dynamics may be approximated by two-dimensional Poiseuille flow as shown in Fig. 1. Due to the presence of a parabolic distribution of the flow velocity, the degree of deformation and orientation of a cell depends upon the depth measured from the flat surface. Therefore, the simulation requires the knowledge of the relation between deformation/orientation and the shear stress.

According to the photomicrographic studies by Goldsmith (6) and Goldsmith and Marlow (7), the cells in Poiseuille flow behave as follows. (*a*) At a shear stress below 0.1 Nm^{-2}, the cells rotate like rigid disks. (*b*) When the shear stress exceeds 0.1 Nm^{-2}, they are deformed into an ellipsoidal shape and orient with the long axis lying at an angle to the flow direction, and the extent of deformation and orientation increases with the shear stress at least up to 0.3 Nm^{-2}. (*c*) The deformation and the orientation of the red cells are generally analogous to those of liquid drops with the flat surface of the deformed cell facing the wall of the tube as do the deformed liquid drops (7). A similar phenomenon was also observed by Fischer et al.

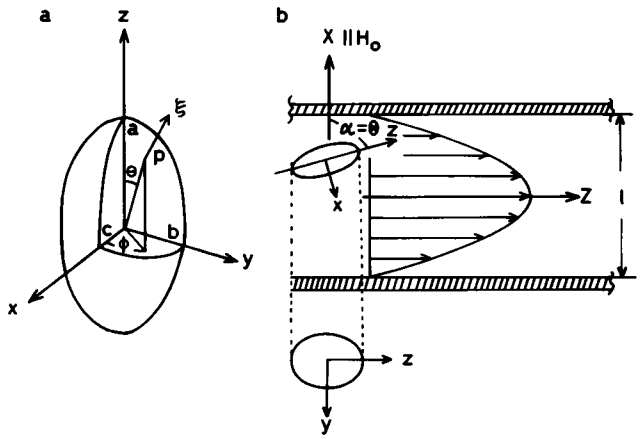

FIGURE 1 Schematic model for deformation and orientation of a red blood cell in a two-dimensional Poiseuille flow. (*a*) The shape of the deformed cell is described by an ellipsoid having three different axial lengths *a*, *b*, and *c*. ξ is the principal axis of the $2p_\pi$ orbital of the spin label at a point *p* on the cell surface. (*b*) The cell orients with the *y* axis of the ellipsoid parallel to the *Y* axis of the ESR cell. The orientation angle α is defined as the one between the *X* and the *z* axis. *l* is the gap between the flat surfaces (l = 0.27 mm) of the flow cell. The arrows parallel to the *Z* axis indicate the parabolic distribution of the flow velocity.

(9, 10) by using a rheoscope, and by Kon et al. by photomicrography (4).

In theoretical study, on the other hand, Richardson (11) calculated the deformation and orientation of an ellipsoidal microcapsule suspended in flow at low shear rates neglecting the influence of the internal fluid. Kholeif and Weymann (12) proposed a two-dimensional model to explain the rotation and deformation of the red cells assuming a fixed shape resembling the actual cross section of an undeformed red cell. Both of these, however, have obvious shortcomings and are not adequate for our purpose. Barthes-Biesel (13) recently proposed a theory on the deformation and orientation, in shear flow, of a microcapsule that consists of a thin elastic spherical membrane enclosing an incompressible Newtonian viscous fluid. Except for the spherical shape chosen, this model is closer in structure to a red cell and may be potentially useful in determining how deformation and orientation of a red cell depends upon the visco-elastic properties of the cell constituents. However, there is a critical discrepancy between the result of calculation and the actual behavior of red cells, especially at high shear rates; namely, the deformation of red cells in shear flow is known to approach a plateau at sufficiently high shear rates, but no such asymptotic behavior could be derived from the calculation. Thus no truly satisfactory theory has yet been proposed to describe the behavior of red cells in shear flow.[1]

In view of this circumstance, we adopt, as a first approximation, the theory for drop deformation developed by Cox (15), which later was expanded by Flumerfelt (16). As will be shown, the description of deformation and orientation derived from the Cox theory can reproduce the above-mentioned behavior of red cells in flow better than the microcapsule models.

The measure of deformation used in the Cox theory is the deformation index, *D*, defined by $D = (L - B)/(L + B)$, where *L* and *B* are the lengths of the long and short deformed axes, respectively, while the third axis is assumed to remain the same as the radius of the original sphere. *D* is related to other parameters appearing in the Cox theory by

$$D = 5(19\lambda + 16)/4(\lambda + 1)[(19\lambda)^2 + (20k/G)^2]^{1/2} \quad (1)$$

where

$$\lambda = \eta_0/\eta \text{ and } k = \sigma/\eta a \ (k \text{ in } s^{-1}). \quad (2)$$

η_0 is the drop viscosity, η, the viscosity of the suspending fluid; σ, the interfacial tension; *a*, the radius of the drop; and *G*, the shear rate. *D* is plotted as a function of *G* in Figs. 2 and 3. The orientation angle α between the longest

[1] After this writing, an improved treatment by Keller and Skalak of the motion of an ellipsoidal membrane encapsulating a Newtonian fluid in plane shear flow came to our attention (14).

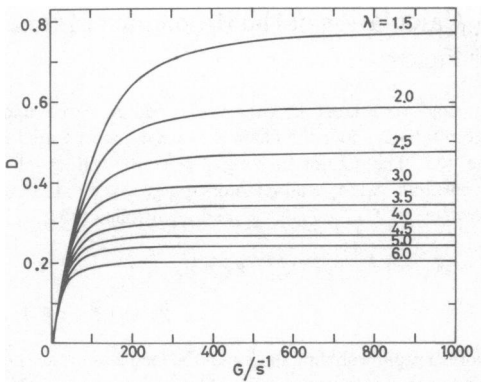

FIGURE 2 The dependence of the deformation index, D, on the shear rate, G, for various values of λ at a fixed $k = 200$ as derived from Eq. 1.

axis of the cell and the normal to the flow direction is given by

$$\alpha = \pi/4 + (1/2)\tan^{-1}(19\lambda G/20k). \quad (3)$$

The dependence of α on G is shown in Fig. 4 for various values of λ. Despite the fact that a large deformation of red cells should, strictly, be outside the range of validity of the theory, the D vs. G profiles derived from Eq. 1 reproduce the qualitative features of the experimental curves by Fischer et al. (9, 10) obtained by using a rheoscope or those of Mohandas et al. (17) by ektacytometry. The profiles also resemble the ESR spectral change vs. G curves obtained by the present authors (2). This is probably due to the fact that despite the biconcave shape of the red cells at rest, the deformed shape is nearly ellipsoidal because the nonspherical part of the initial shape is transient and is eliminated under shear stress in a short period of time, as pointed out by Cox (15). In fact, microscopic observations at high shear stress values support this interpretation (18, 19).

In applying the Cox theory we treat λ and k as adjustable parameters to find the best-fitted simulation spectra, disregarding, at first, the original physical meanings. We extract a semi-empirical relationship between the observed spectral change and the cell deformation index D. We will

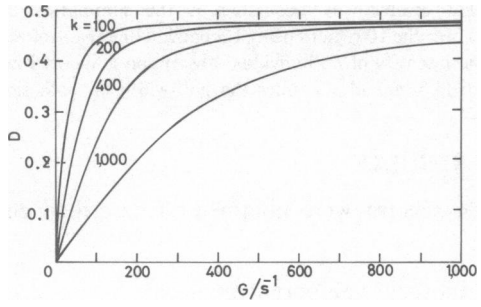

FIGURE 3 The dependence of the deformation index, D, on the shear rate, G, for various values of k at a fixed $\lambda = 2.5$ as derived from Eq. 1.

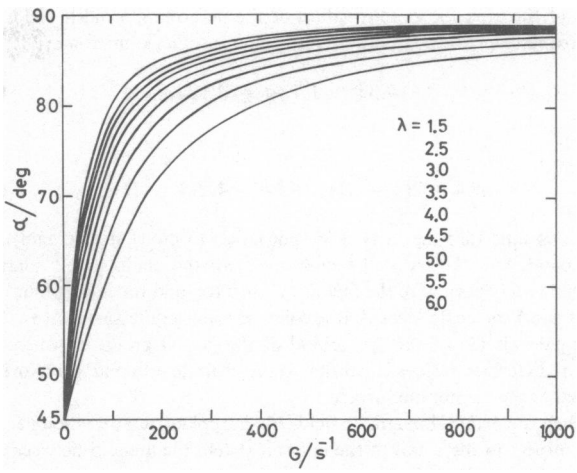

FIGURE 4 The dependence of orientation angle α on G for various values of λ at a fixed $k = 200$ as derived from Eq. 3.

show that the estimated maximum deformation index is in good agreement with the experimental values and demonstrate that our model for the behavior of the red cells in shear flow is an adequate first approximation.

THEORY

Shear Rate in ESR Cell

We assume that shear rate, G, depends upon the depth, x, measured from the flat surface of the flow cell and follows the relation for fully developed Newtonian laminar flow (9):

$$G = 12V(0.5 - x/l)/(l^2w), \quad (4)$$

where l is the gap ($l = 0.27$ mm) between the flat surfaces, V is the volume flow rate, and w is the width (0.8 cm) of the ESR cell. The shear stress is estimated from G and the viscosity of the red cell suspension at 35% hematocrit in a 5% dextran solution. The viscosity is assumed to be constant at 0.89×10^{-2} Nsm^{-2}. Half of the gap l is divided into 10 regions, and the values of G, the orientation angle, α, and the deformation index, D, were calculated for each of the regions.

Cell Shape

We assume the shape of the deformed cell to be an ellipsoid having three unequal axial lengths

$$x^2/a^2 + y^2/b^2 + z^2/c^2 = 1 \quad (5)$$

as shown in Fig. 1. We define the deformation index for the red cell, as in the theory by Cox (14), in terms of the deformed axes for which we choose a and b (Fig. 1). Thus, $D = (a - b)/(a + b)$. This choice of deformed axes differs from that for the liquid drop in which the deformed axes (L, B) lie in the plane perpendicular to the flat flow cell surface. The difference is an inevitable consequence of the different initial shapes of the liquid drop (sphere) and the red cell (discoid). This choice of the deformed axes is not only reasonable in view of the aforementioned photomicrographic observations, but it also fulfills the requirement that $D \to 0$ as the shear rate tends to 0 (Eq. 1). The value of c is estimated using a constraint that the surface area of the red cell remains constant (142 μm^2) throughout the range of deformation (21). Numerical calcula-

tions of the area for various values of the deformation index yields an approximate quadratic equation[2] for c in terms of a (in micrometers):

$$c = 4.31 - 1.13a + 0.123a^2 \quad (6)$$

where

$$a = 4.2(1 + D), \text{ and } b = 4.2(1 - D). \quad (7)$$

We assume that the fatty acid spin labels (5-doxyl stearic acid) are incorporated in the red cell membrane with the chain length aligned approximately normal to the membrane surface, and the hydrophilic end of the label molecule located at a point (r, θ, ϕ) on the surface (8). The principal axis (ξ) of the $2p_\pi$ orbital of the N—O group in which the unpaired electron resides is parallel to the chain length and, therefore, is normal to the membrane surface.

When the external magnetic field, H_0, is applied at a direction (Θ, Φ) with respect to the z axis of the ellipsoidal cell, the angle β between the field and ξ at (r, θ, ϕ) on the surface is given by

$$\cos\beta = (bc \sin\theta\cos\phi \sin\Theta\cos\Phi)/aQ + (ac \sin\phi \sin\Theta\cos\Phi)/bQ + (ab\cos\theta\cos\Theta)/cQ \quad (8)$$

where

$$Q = [(bc\sin\theta\cos\phi)^2/a^2 + (ac\sin\theta\sin\phi)^2/b^2 + (ab\cos\theta)^2/c^2]^{1/2}. \quad (9)$$

The angle β is calculated numerically from Eq. 8. Assuming that the fatty acid spin labels are uniformly distributed in the membrane of the cell, the population around a point $p(r, \theta, \phi)$ may be proportional to the surface area dS

$$dS = [r^2\sin^2\theta + \sin^2\theta\,(\partial r/\partial\theta)^2 + (\partial r/\partial\phi)^2]^{1/2} r d\theta d\phi = Q\sin\theta\, r^4 d\theta d\phi/abc \quad (10)$$

and

$$r = [(\sin\theta\cos\phi/a)^2 + (\sin\theta\sin\phi/b)^2 + (\cos\theta/c)^2]^{-1/2}. \quad (11)$$

Consequently, the intensity of the ESR signal due to the spin labels around the point p is also proportional to dS.

Cell Orientation in Shear Flow

The longest axis of the deformed cell tends to orient along the flow direction with the flat surface facing the flow cell wall. Since the external magnetic field is applied normal to the flat cell in our experiments (2–4), the orientation angle α coincides with Θ as shown in Fig. 1. We also assume that at a shear stress below 0.05 Nm^{-2}, the red cells are randomly oriented. Although, strictly, red cells tumble like rigid disks in shear flow below 0.05 Nm^{-2} shear stress, and the tumbling is not random (6), this assumption is justified since completely hardened red cells show little ESR spectral change in flow.

[2] The approximation of Eq. 6 was tested by computing the surface area using the more accurate expression given by Keller and Skalak (Eq. 69 of reference 14; typographical error corrected). For $b \geq c$, the axial lengths obtained from Eqs. 6 and 7 give the surface area $S = 141 \pm 2\ \mu m^2$, which is in good agreement with the constraint. Incidentally, the cell volume, which is not constrained here, is similarly calculated to be $121 \pm 4\ \mu m^3$, a little larger than the actual cell volume.

Calculation of the Resonance Magnetic Fields

The fatty acid spin label is known to undergo rapid and random anisotropic rotations about the chain axis when incorporated in the cell membrane (8). The motion averaged principal values of hyperfine coupling constants, $A_\parallel$, $A_\perp$, and g factors, $g_\parallel$, $g_\perp$, are related to the single crystal parameters, T_x, T_y, T_z, g_x, g_y, and g_z, as follows (8):

$$A_\parallel = T_z, \quad A_\perp = (T_x + T_y)/2, \quad g_\parallel = g_z, \quad g_\perp = (g_x + g_y)/2. \quad (12)$$

Furthermore, a rapid wobbling motion of the long axis of the rotating spin label must be taken into account (8). The wobbling averaged magnetic parameters $A_\parallel$, $A_\perp$ are

$$A_\parallel^w = A\perp + (A_\parallel - A_\perp)W,$$
$$A_\perp^w = A_\perp + (A_\parallel - A_\perp)(1 - W)/2 \quad (13)$$

where

$$W = (1 + \cos\gamma + \cos^2\gamma)/3, \quad (14)$$

and γ is the maximum half amplitude of wobbling. Corresponding expressions hold for the g factors. The reasonant magnetic field $H(J, \beta)$ is calculated by the following equations:

$$H(J, \beta) = h[\nu + JA(\beta)]/g(\beta)\beta_e, \quad (15)$$

$$A(\beta) = [(A_\parallel^w\cos\beta)^2 + (A_\perp^w\sin\beta)^2]^{1/2}, \quad (16)$$

$$g(\beta) = g_\parallel^w\cos^2\beta + g_\perp^w\sin^2\beta, \quad (17)$$

where h is the Planck's constant; ν, the microwave frequency; β_e, the Bohr magneton; and J is the nuclear quantum number of ^{14}N in the N—O group.

Calculation of the Line Width

It is known that the line width of the absorption depends upon the ^{14}N nuclear quantum number $(+1, 0, -1)$ and the angle β between the external magnetic field and the z axis of the nitroxide group (21)

$$W(+1, \beta) = 3.0 \quad (18)$$

$$W(0, \beta) = 2.5 + 1.8(3\cos^2\beta - 1)^2/4 \quad (19)$$

$$W(-1, \beta) = 4.0 \text{ (in gauss)}. \quad (20)$$

Convolution of the Stick Spectra

A simulated spectrum is calculated as the summation of all the histograms over the 10 regions using Lorentzian line shape of varying line widths. The intensity of an individual absorption is ignored beyond the magnetic field range of six times the half-width on both sides of the peak.

RESULTS

The ESR spectra were obtained as described elsewhere (2).

Isotropic Spectrum

First, the wobbling angle, γ, was estimated to be 35° from the best fit of an observed spectrum at rest. The calculated

and the observed spectra are compared in Fig. 6 a. The numerical values used for other magnetic parameters were taken from reference 21. They are all assumed to be constant throughout the flow process.

Simulation of Anisotropic Spectra

We simulated five observed spectra measured at different shear stress values by adjusting only two parameters, λ and k. The dependences of the deformation index D and G in Figs. 2 and 3 show that the value of D at the plateau depends mostly on λ and is virtually independent of k for the range of $k < 500$, whereas the dependency of D on G before the plateau is reached is mainly determined by k. Since, as mentioned above, there is a close resemblance between D vs. G curves and the spectral change vs. G profiles, the values of λ and k may be estimated by using the characteristics of the ESR spectral change at a high and a low shear rate, respectively.

For that purpose, we adopt the ratio l'/l of the peak-to-trough amplitudes of the low field and the center absorptions as shown in Fig. 6 *f*. Generally, the greater the degree of deformation and orientation of red cells, a larger value for l'/l is expected. Fig. 5 shows the dependence of the calculated l'/l on λ under a sufficiently high shear stress of 8 Nm^{-2} (shear rate ~ 900 s^{-1}) at the flow cell surface when k is fixed at 200. Despite that the decrease in λ should cause increase in D (meaning a larger cell deformation) as can be seen in Fig. 2, the calculated l'/l is seen to decrease with decrease in λ. This apparent reversed trend can be understood if we realize that according to Eq. 3, at the shear stress of 8 Nm^{-2}, the cells are almost completely oriented even though the λ values may be relatively large and the cells are not greatly deformed (see Fig. 4). In this hypothetical situation, since the large flat area of the cell is normal to the magnetic field, and the population of the spin label at the flat surface is much higher than on the rim, the calculated l'/l value is excessively large (see Fig. 2, reference 5). As the λ value is decreased and the cells are deformed accordingly, to approach a more realistic situation, l'/l decreases because of the decrease in the flat portion of the cell surface normal to the magnetic field and the corresponding increase in the surface area on the rim. Thus, by choosing l'/l equal to the experimentally observed value, the optimal degree of deformation and orientation can be determined.

From the observed l'/l of 0.58 at the shear stress of 8 Nm^{-2}, λ is estimated to be 2.72. Fig. 5 also shows the relationship of l'/l and k at a low shear stress of 0.4 Nm^{-2} with λ fixed at 2.72. Again, using the observed l'/l of 0.43, k is determined to be 280.

The simulated spectra using these parameter values are compared in Fig. 6 with the observed ones at various shear rates. The values of l'/l obtained by simulation are compared with the observed values in Table I. The excellent agreement between them verifies that the assumptions

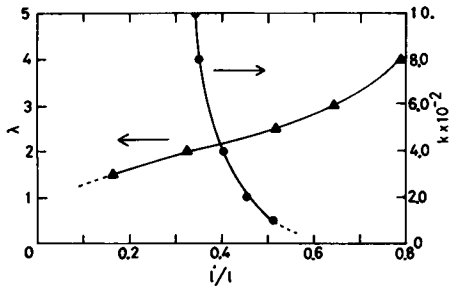

FIGURE 5 The relation of the calculated spectral parameter, l'/l, to λ at the shear stress of 8.0 Nm^{-2} (*left* ordinate) at $k = 200$, and a similar relation to k at the shear stress of 0.4 Nm^{-2} (*right* ordinate) with $\lambda = 2.72$.

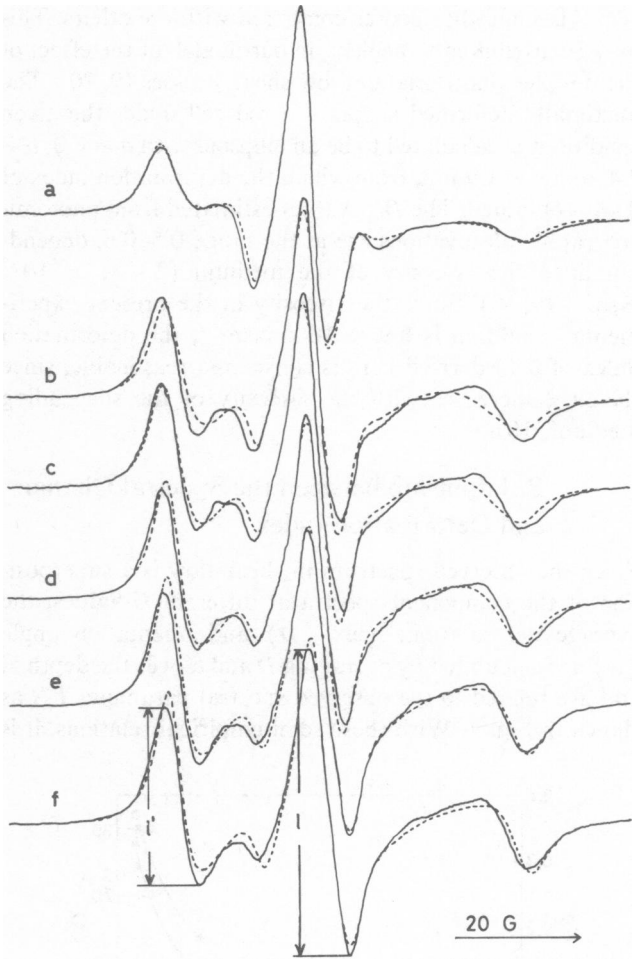

FIGURE 6 Comparison of the simulated spectra with the corresponding observed ones. Simulated spectra (– – –) were calculated with the following parameters: $g_x = 2.0088$, $g_y = 2.0061$, $g_z = 2.0027$; $T_x = 17.6$, $T_y = 16.73$, $T_z = 93.8$ (in megahertz); $\gamma = 35°$, $\lambda = 2.72$, $k = 280$. The observed spectra (——) were obtained at 25°C from a red cell suspension at 35% hematocrit in a 5% dextran solution in 5 mM isotonic phosphate buffer (pH = 7.4). The flow rate was adjusted to give the shear stress at the surface of the flow cell (*a*) 0.0, (*b*) 0.3, (*c*) 0.4, (*d*) 1.0, (*e*) 3.2, and (*f*) 8.0 Nm^{-2}.

TABLE I
COMPARISON OF THE OBSERVED l'/l VALUES WITH THOSE ESTIMATED FROM THE SIMULATED SPECTRA

Shear stress	Observed*	Simulated
Nm^{-2}		
0	0.19	0.19
0.3	0.42	0.36
0.4	0.46	0.45
1.0	0.52	0.53
3.2	0.57	0.58
8.0	0.58	0.58

*Experimental error ± 0.01.

made concerning the deformation and orientation are a good approximation. The fit at a low shear stress of 0.3 Nm^{-2} is somewhat poorer compared with the others. This may be attributed to neglect, in our model, of the effect of the dimples that remain at low shear stresses (9, 10). The maximally deformed shape of a red cell under the given conditions is calculated to be an ellipsoid with $a = 6.0$, $b = 2.4$, and $c = 1.9$ μm, from which the deformation index of 0.44 is obtained. The D_{max} values estimated from photomicrographic observations are in the range 0.5–0.6, depending upon the viscosity of the medium $(2 \sim 3) \times 10^{-2}$ Nsm^{-2} (9, 10). Since the viscosity in the present experimental condition is 8.9×10^{-3} Nsm^{-2}, the deformation index of 0.44 derived here is considered reasonable, since the D_{max} increases with the viscosity of the suspending medium (10).

Relationship between the Spectral Change and Deformation Index

Since the observed spectrum in shear flow is a superposition of the component spectra at different G values, the average deformation index $\langle D \rangle$ and orientation angle $\langle \alpha \rangle$ are calculated by averaging D and α over the depth x, and are related to the observed spectral parameter l'/l as shown in Fig. 7. With these semi-empirical relations, it is possible to estimate both the average deformation index and orientation angle from the observed ESR spectra of spin-labeled intact red cells at a given shear rate.

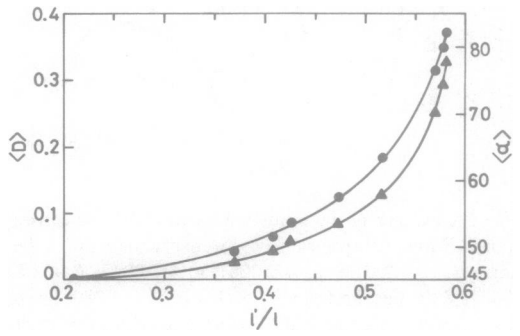

FIGURE 7 The relation of the average deformation index $\langle D \rangle$ (*left* ordinate, ●) or the average orientation angle $\langle \alpha \rangle$ (*right* ordinate, ▲) with the spectral parameter, l'/l, calculated with $\lambda = 2.72$ and $k = 280$. The shear stress is changed as in Fig. 6.

DISCUSSION

We have shown in our previous papers that the change in the ESR spectra of the red cells under shear stress is closely associated with both deformation and orientation of the cells (2–4). Here we have derived semi-empirical relationships of a spectral parameter l'/l to the average deformation index or to the average orientation angle. Although the theory used for constructing a model for the behavior of the red cells in flow is admittedly an approximation, it provides an insight into some aspect of the red cell behavior in flow. The satisfactory agreement between the simulated and the observed spectra in the present work implies that our model of the red cells in flow based upon the Cox theory for drop deformation indeed describes some of the essential features of the red cell behavior. A further confirmation of this is that all six spectra taken under various shear stresses can be reproduced using a single set of λ and k values, and that the fit is especially sensitive to the change of λ value (see Fig. 5).

In this treatment, we used λ and k simply as adjustable parameters, independent of their original meanings of the relative viscosity of the intra- and extra-cellular fluids and the quantity related to the interfacial tension, respectively. Note, however, that the dependence of D vs. G curves upon the parameter λ derived from Eq. 1 (Fig. 2) resembles the ESR spectral change vs. G curves observed when the red cells were treated to various degrees by glutaraldehyde (2). The profile is also similar to the deformation index vs. G plot of the red cells in hypotonic media observed by ektacytometry (17). In both treatments, the whole cell deformability is modified by, among other factors, the change in the intracellular fluid viscosity through cross-linking by glutaraldehyde or due to dilution in hypotonic media.

The appearance of the D vs. G plot (Fig. 3) shows a characteristic dependence on k such that there is a greater decrease in D in the low shear rate region as k is increased, and the decrease in D becomes insignificant in the high shear region. This is especially evident when $k < 500$. The particular trend has been observed experimentally in the deformation index vs. G curves when red cells were exposed to heat treatment at 47° for various lengths of time (17) or when the cells were treated by diamide (9). The main effect of the treatments is the reduced membrane deformability. Thus, the parameters λ and k seem to play, in the present model, the roles analogous to their original meanings.

Since $\eta_0 \sim 10^{-2}$ Nsm^{-2} (23–25) and η for a 5% dextran solution is 3×10^{-3} Nsm^{-2}, the ratio λ is 3.3 and as determined in this simulation, λ is 2.7. These values are in fair agreement.

Estimation of the surface tension σ is not straightforward, since $k = \sigma/\eta a = 280$ was determined from the ESR spectral characteristics that represent the average over the distribution of the degrees of orientation and deformation. Goldsmith and Marlow (7) estimated the surface tension of the red cells at the shear stress of 0.1 Nm^{-2} from the deformation data to be 1.4×10^{-5} Nm^{-1}. In the present work, assuming that $a = 4.2$ μm (Eq. 7), $k = 280$ gives $\sigma = 0.35 \times 10^{-5}$ Nm^{-1}, which is one-fourth of their estimation. The discrepancy is not unexpected in view of the approximations in the theory. The numerical values determined in this simulation should be noted with caution, especially since the whole cell deformation/orientation is a complex event, which is determined also by factors other than the single cell deformability.

The authors are indebted to Dr. Richard S. Chadwick and Dr. Aydin Tözeren for their critical comments and stimulating discussions on the manuscript.

Received for publication 1 December 1983 and in final form 20 April 1984.

REFERENCES

1. Rice-Evans, C. A. and M. J. Dunn. 1982. Erythrocyte deformability and disease. *Trends Biochem. Sci.* 7:282–286.
2. Noji, S., F. Inoue, and H. Kon. 1981. Spin label study of erythrocyte deformability. I. Electron spin resonance spectral change under shear flow. *Blood Cells.* 7:401–411.
3. Noji, S., F. Inoue, and H. Kon. 1981. Use of spin label and the flow induced ESR spectral difference for studying erythrocyte deformation. *J. Biochem. Biophys. Methods.* 5:251–258.
4. Kon, K., S. Noji, and H. Kon. 1983. Spin label study of erythrocyte deformability. III. Further characterization of electron spin resonance spectral change in shear flow. *Blood Cells.* 9:427–441.
5. Bitbol, M., and F. Leterrier. 1982. Measurement of erythrocyte orientation in a flow by spin labeling. *Biorheology.* 19:669–680.
6. Goldsmith, H. L. 1971. Deformation of human red cells in tube flow. *Biorheology.* 7:235–242.
7. Goldsmith, H. L., and J. Marlow. 1972. Flow behaviour of erythrocyte I. Rotation and deformation in dilute suspensions. *Proc. R. Soc. Lond. B. Biol. Sci.* 182:351–384.
8. Griffith, O. H., and P. C. Jost. 1976. Lipid spin labels in biological membranes. *In* Spin Labeling I. L. J. Berliner, editor. Academic Press, Inc., New York. 454–519.
9. Fischer, T. M., C. W. M. Haest, M. Stöhr, D. Kamp, and B. Deuticke. 1978. Selective alteration of erythrocyte deformability by SH reagents. *Biochim. Biophys. Acta.* 510:270–282.
10. Fischer, T., and H. Schmid-Schönbein. 1978. Tank tread motion of red cell membranes in viscometric flow. Behaviour of intra-cellular and extracellular marks (with film). *In* Red Cell Rheology. M. Besis, S. B. Shohet, and N. Mohandas, editors. Springer-Verlag. Berlin-Heidelberg-New York. 347–358.
11. Richardson, E. 1974. Deformation and haemolysis of red cells in shear flow. *Proc. R. Soc. Lond. Sect. A.* 338:129–153.
12. Kholeif, I. A., and H. D. Weymann. 1974. Motion of a single red blood cell in plane shear flow. *Biorheology.* 11:337–348.
13. Barthes-Biesel, D. 1980. Motion of a spherical microcapsule freely suspended in a linear shear flow. *J. Fluid Mech.* 100:831–853.
14. Keller, S. R., and R. Skalak. 1982. Motion of a tank-treading ellipsoidal particle in a shear flow. *J. Fluid Mech.* 120:27–47.
15. Cox, R. G. 1969. The deformation of a drop in a general time-dependent fluid flow. *J. Fluid Mech.* 37:601–623.
16. Flumerfelt, R. W. 1980. Effects of dynamic interfacial properties on drop deformation and orientation in shear and extensional flow fields. *J. Colloid Interface Sci.* 76:330–349.
17. Mohandas, N., M. R. Clark, M. S. Jacobs, and S. B. Shohet. 1980. Analysis of factors regulating erythrocyte deformability. *J. Clin. Invest.* 66:563–573.
18. Sutera, S. P., and M. H. Mehrjardi. 1975. Deformation and fragmentation of human red blood cells in turbulent shear flow. *Biophys. J.* 15:1–10.
19. Allard, C., N. Mohandas, and M. Bessis. 1978. Red cell deformability change in hemolytic anemias estimated by diffractometric methods (ectacytometry). *In* Red Cell Rheology. M. Bessis, S. B. Shohet, and N. Mohandas, editors. Springer-Verlag. Berlin-Heidelberg-New York. 209–220.
20. Fox, R. W., and A. T. McDonald. 1973. Introduction to Fluid Mechanics. John Wiley and Sons, Inc., New York. 334–339.
21. Fung, Y. C. B., and P. Tong. 1968. Theory of the sphering of red blood cells. *Biophys. J.* 8:175–198.
22. Gaffney, B. J., and H. M. McConnell. 1974. The paramagnetic resonance spectra of spin labels in phospholipid membranes. *J. Magn. Reson.* 16:1–28.
23. Cokelet, G. R., and H. J. Meiselman. 1968. Rheological comparison of hemoglobin solutions and erythrocyte suspensions. *Science (Wash. DC).* 162:275–277.
24. Chien, S., S. Usami, and J. F. Bertles. 1970. Abnormal rheology of oxygenated blood in sickle cell anemia. *J. Clin. Invest.* 49:623–634.
25. Hochmuth, R. M., K. L. Buxbaum, and E. A. Evans. 1980. Temperature dependence of the viscoelastic recovery of red cell membrane. *Biophys. J.* 29:177–182.